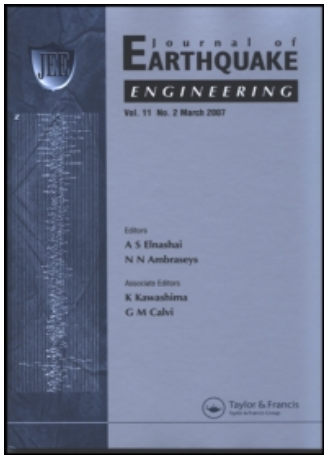

Journal of Earthquake Engineering
Publication details, including instructions for authors and subscription information:
http://www.informaworld.com/smpp/title~content=t741771161

Effective Cyclic Energy as a Measure of Seismic Demand

Online Publication Date: 01 September 2007
To cite this Article: Kalkan, Erol and Kunnath, Sashi K. (2007) 'Effective Cyclic Energy as a Measure of Seismic Demand', Journal of Earthquake Engineering, 11:5, 725 - 751
To link to this article: DOI: 10.1080/13632460601033827
URL: http://dx.doi.org/10.1080/13632460601033827

Journal of Earthquake Engineering, 11:725–751, 2007

ISSN: 1363-2469 print / 1559-808X online
DOI: 10.1080/13632460601033827

Taylor & Francis
Taylor & Francis Group

Effective Cyclic Energy as a Measure of Seismic Demand

EROL KALKAN and SASHI K. KUNNATH

Department of Civil and Environmental Engineering, University of California, Davis, California, USA

Structural damage during strong ground shaking is associated with both the seismic input energy and the ability of structural components to dissipate energy through viscous damping and inelastic cyclic response. The correlation of the damage potential of ground motions with seismic energy demand is an important element in developing energy-based design methodologies. This article proposes a new measure of the severity of ground motions by introducing the concept of effective cyclic energy (ECE) defined as the peak-to-peak energy demand (sum of hysteretic and damping energies) imposed on a structure over an effective duration that is equivalent to the time between two zero-crossings of the "effective velocity pulse." The proposed energy measure, which is dependent on the characteristics of the ground motion, is shown to be well correlated with peak seismic demand for a range of system parameters. The development of ECE also provides a basis for defining a non dimensional response index (γ_{eff}) to quantify the destructive potential of ground motions. The effectiveness of the new index parameter is validated using an extensive set of near-fault accelerograms and also compared to other ground motion severity indices. Finally, ECE demand of a MDOF system is estimated through modal-energy-decomposition of elastic and inelastic SDOF systems, and the concept of ECE spectrum is proposed to estimate the modal target energy demands for performance evaluation of structures.

Keywords Input Energy; Cyclic Energy; Severity Index; Seismic Demand; Near-Fault Records

1. Introduction

A fundamental precept in performance-based seismic design (PBSD) is to ensure that structural components have adequate ductility and energy dissipation capacity so that the expected damage in terms of story drift and/or member deformations can be controlled to lie within the limits of desired performance states. While the correlation of demand measures to performance states remains a central issue in PBSD, the estimation of expected demand in relationship to ground motion characteristics can be viewed as an important first step in the process.

Various approaches to seismic design have evolved following the recognition that traditional force-based procedures are generally unsatisfactory in the context of PBSD. These include the development of displacement-based design methods and so-called energy-balance formulations wherein the energy imparted to the structure by the earthquake is balanced by providing adequate energy dissipation capacity. Energy-based procedures can also form the basis of estimating expected seismic demands and thereby indirectly assess the destructive potential of ground motions. Examples of methodologies,

Received 19 January 2006; accepted 31 August 2006.
Address correspondence to Dr. Erol Kalkan, (currently at California Geological Survey, Earthquake Engineering Program); E-mail: Erol.Kalkan@conservation.ca.gov

which have evolved from considerations of input and dissipated energy include the procedures proposed by Fajfar [1992], Teran-Gilmore [1998], Decanini and Mollaioli [2001] and Riddell and Garcia [2001]. While these procedures utilize either absolute or relative energy measures, they do not account for possible variations of energy formulations selected according to ground motion characteristics.

For ordinary far-fault records, it is now well recognized that structural damage depends not only on the maximum deformation but also the contribution of low-cycle fatigue effects [Fajfar and Vidic, 1994; Kunnath and Chai, 2004; Sucuoglu and Erberik, 2004; Teran-Gilmore and Jirsa, 2005]. On the other hand, most of the damage caused by near-fault records is a result of instantaneous energy demand associated with intense pulse effects and few plastic cycles [Kalkan and Kunnath, 2006a]. In this case, low-cycle fatigue effects are less significant and structural damage is directly related to peak seismic demands.

In addition, typical near-fault records characterized by fling or forward-directivity contain long period velocity pulses produced either by the integration of apparent acceleration pulses or a succession of high frequency acceleration peaks. Figure 1 displays the acceleration and velocity time-series of representative near-fault ground motions. Notably, the Rinaldi Receiver Stn. record exhibits a distinguishable acceleration pulse (see the window), whereas the Sakarya record does not. The difference in the initiation of velocity pulse has been shown to influence the imparted energy to structural systems [Kalkan and Kunnath, 2007a]. As such, records having apparent acceleration pulses produce instantaneous energy spikes in the early phase of response, which can be appreciably larger than the energy accumulated at the end. Conversely, for near-fault records characterized by high-frequency acceleration spikes, input energy tends to accumulate progressively over time resembling typical cyclic far-fault records. It has been also shown that severity of these energy spikes depend upon the ratio of system period to the dominant pulse period of the ground motion [for details see Kalkan, 2006; Kalkan and Kunnath, 2007a]. Figure 2 compares relative and absolute energies computed for a typical forward directivity and fling type of motion (both exhibit distinct acceleration pulses) recorded close to the causative fault with those calculated for an ordinary far-fault motion recorded away from the source. The difference in the two energy definitions is apparent in case of near fault records. This discrepancy arises from different definitions of kinetic energy (i.e., $E_K^{'}$ vs. E_K), used in relative ($E_I^{'}$) and absolute (E_I) energy computations while damping and strain

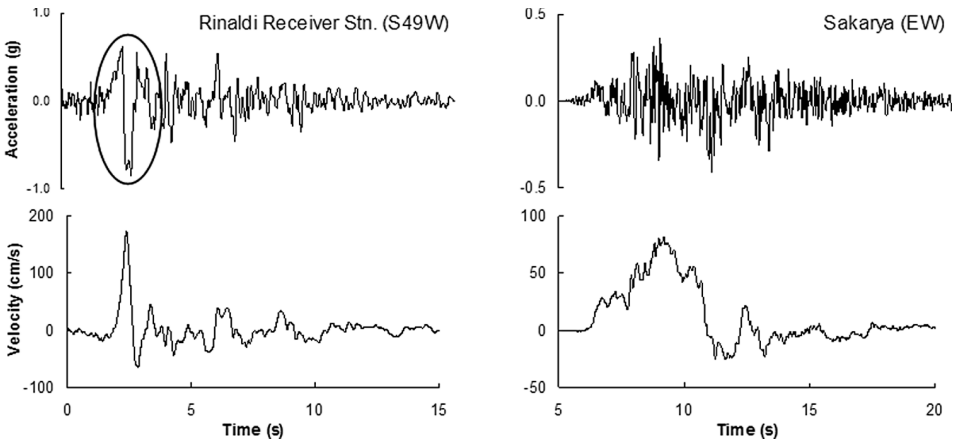

FIGURE 1 Earthquake recordings having apparent acceleration pulse (left), and packed with random high frequency acceleration spikes (right).

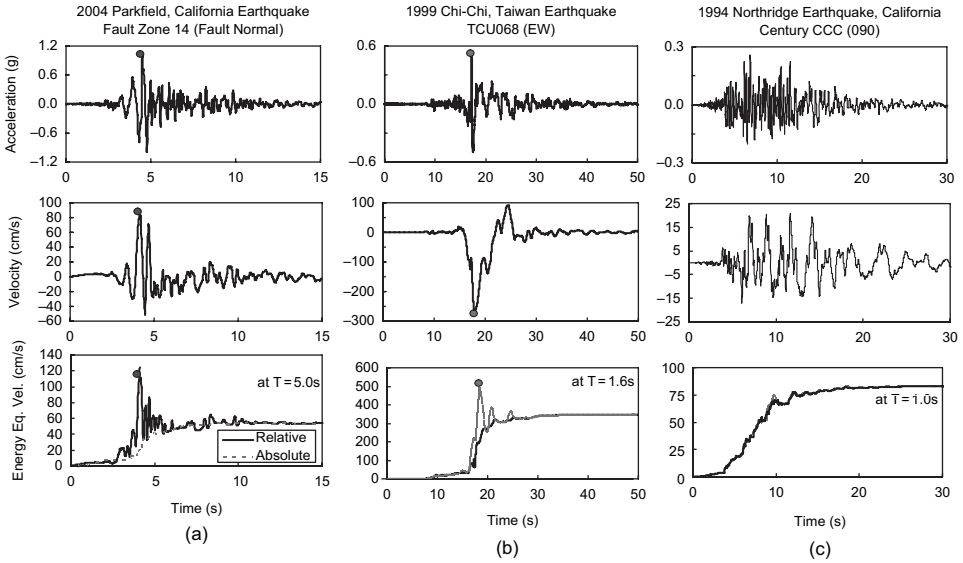

FIGURE 2 Comparison of absolute and relative energies computed for a SDOF elastic oscillator excited by (a) near-fault forward directivity, (b) near-fault fling and, (c) far-fault recordings.

energy (i.e., hysteretic energy) terms remain identical in both formulations. Hence, the difference can be written as:

$$E_I - E_I' = E_K - E_K' = \frac{1}{2} m\dot{u}_g^2 + m\dot{u}_g\dot{u}. \tag{1}$$

The right-hand side of Eq. 1 has two terms, the former is the kinetic energy due to ground velocity, while later is the work done by ground acceleration ($m\ddot{u}_g$) on the respective incremental system displacement (du). If we ignore the contribution of $m\dot{u}_g\dot{u}$, then absolute energy should be always greater or at least close (depends on the intensity of ground motion velocity) to its relative counterpart regardless of system oscillation period. However, the last term (i.e., $m\dot{u}_g\dot{u}$), which relates the phase difference between ground movement and structural response may significantly increase the energy difference if it has a positive sign (i.e., in-phase response with respect to ground movement) or diminish the energy difference if it has a negative sign (out-of-phase response with respect to ground movement).

This noticeable difference in relative or absolute energies (as demonstrated in Figure 2) brings additional complexity and uncertainty in selection of appropriate energy measures to characterize the destructive power of near-fault accelerograms. This article, therefore, aims to quantify the intensity and spectral distribution of energy demand, and express this demand as a function of ground motion characteristics and of the earthquake resisting system while being independent of the manner in which input energy is defined. Towards this objective, a comprehensive set of near-fault records were compiled and a systematic evaluation of a range of inelastic SDOF systems was carried out. A careful evaluation of computed seismic demands has led to the development of a new measure of the severity of ground motions to be referred to as the "Effective Cyclic Energy" (ECE). The correlation of ECE to peak displacement demand was verified through inelastic SDOF response

history analyses considering different force-deformation behavior (hysteretic models) at constant ductility levels. Based on the conceptual development of ECE, a non dimensional ground motion severity index (γ_{eff}) is proposed. The validity and stability of γ_{eff} are systematically compared with other response indices using a wide range of ground motion data to account for aleatoric variability in earthquake recordings.

Finally, the ECE demand of a MDOF system is estimated using the proposed modal-energy-decomposition for elastic and inelastic SDOF systems. The concept of ECE spectrum is next introduced to estimate the modal target energy demands in MDOF systems to be directly used in performance evaluation of structures.

2. Near-fault Ground Motion Dataset

Table 1 lists all the records used in the study, and Figure 3 demonstrates the distribution of their PGA (peak-ground-acceleration) with respect to moment magnitude (M_W) and closest fault distance viz., closest distance to the surface projection of the fault [i.e., r_{jb} see Boore *et al.*, 1997]. These ground motions were recorded from earthquakes having a magnitude range from 6.0 to 7.6 and at distances varying from 0.0 to 17.0 km to the causative fault. The records either contain forward-directivity or fling; fling records in Table 1 were processed by baseline correction only (by fitting high order segmental polynomials) following the removal of pre-event mean. Such a scheme is used for correction of raw data since conventional filtering techniques may distort or eliminate the true static displacement at the end of the time-history. Accordingly, the shape of the major velocity pulse may change, hence the true energy content may totally be different. The information on true static offsets was retrieved from the available GPS measurements. The applied correction scheme guarantees that the velocity will be zero near the beginning and at the end of the time-series [see Kalkan and Kunnath, 2006a for details of applied correction scheme]. All of the selected recordings contain long-period velocity pulses as characteristic of near-fault accelerograms influenced by fling or forward-directivity (see Figure 2). Near-fault recordings with backward directivity were not included in the database since they generally did not exhibit pulse-like characteristics. The compilation of the dataset, was guided by observations reported in previous studies including Boore [2001]; Chopra and Chintanapakdee [2001]; Mavroeidis and Papageorgiou [2003]; Bray and Rodriguez-Marek [2004]; Kalkan and Gülkan [2004].

3. Relationship between Input Energy and System Response

The feasibility of defining a rational energy-based descriptor that can be related to the severity of earthquake motions and also to critical system demand parameters requires a clear understanding of the effects of seismic input energy on building structures. Therefore, peak displacements of inelastic SDOF systems subjected to an ensemble of near-fault records were compared to seismic input energy. Figure 4 presents the energy, velocity and displacement time history, and the resulting force-deformation response computed for an inelastic SDOF oscillator subjected to the near-fault records shown in Figure 1. A bilinear material model with 1% kinematic hardening (see Figure 5a) was used to generate these results for a system with a period of 1.0 s and a ductility ratio (μ) of 4. Damping ratio was taken as 5% of critical (same as for all SDOF systems used in this study). Since the records were not scaled, the yield strength of the systems was adjusted to achieve the desired ductility ratio. In these figures, the energy measure used is the relative input energy (E_I') which is formulated as follows:

TABLE 1 Near-fault earthquake recordings

No.	Year	Earthquake	M_w	Mech.[1]	Station	Near Fault Characteristics	Dist.[2] (km)	Site Class[3]	Data Src.[4]	Comp.	PGA (g)	PGV (cm/s)	PGD (cm)	T_D[5] (s)	V/A[6] (s)
1	1966	Parkfield	6.1	SS	Temblor	Forward-Dir.	11.4	C	1	205	0.36	21.64	3.79	4.35	0.06
2	1966	Parkfield	6.0	SS	Cholame 2WA	Forward-Dir.	6.6	C	1	065	0.48	75.04	22.37	6.99	0.16
3	1971	San Fernando	6.6	TH/REV	Pacoima Dam	Forward-Dir.	2.8	B	1	254	1.16	54.30	11.73	6.72	0.05
4	1978	Tabas	7.4	TH	Tabas	Forward-Dir.	3.0	D	1	TR	0.85	121.43	95.11	16.12	0.15
5	1979	Imperial-Valley	6.5	SS	El Centro Array #3	Forward-Dir.	13.8	D	1	140	0.27	46.84	18.90	11.87	0.18
6	1979	Imperial-Valley	6.5	SS	El Centro Diff. Array	Forward-Dir.	5.6	D	1	270	0.35	71.23	45.90	6.95	0.21
7	1979	Imperial-Valley	6.5	SS	El Centro Imp Co Cent	Forward-Dir.	7.6	D	1	092	0.23	68.80	39.38	13.18	0.30
8	1979	Imperial-Valley	6.5	SS	El Centro Array #4	Forward-Dir.	8.3	D	2	S50W	0.36	80.56	72.00	10.32	0.23
9	1979	Imperial-Valley	6.5	SS	El Centro Array #6	Forward-Dir.	3.5	D	2	S50W	0.44	113.35	72.00	8.24	0.26
10	1979	Imperial-Valley	6.5	SS	El Centro Array #7	Forward-Dir.	3.1	D	2	S50W	0.46	113.30	47.46	4.80	0.25
11	1979	Imperial-Valley	6.5	SS	El Centro Array #8	Forward-Dir.	4.5	D	1	140	0.60	54.26	32.39	6.79	0.09
12	1979	Imperial-Valley	6.5	SS	El Centro Array #10	Forward-Dir.	8.7	D	2	320	0.23	46.26	26.74	12.02	0.20
13	1979	Imperial-Valley	6.5	SS	Bonds Center	Forward-Dir.	4.4	D	1	140	0.59	45.22	16.80	9.66	0.08
14	1979	Imperial-Valley	6.5	SS	Holtville Post Office	Forward-Dir.	8.8	D	1	225	0.25	48.76	31.63	11.82	0.20
15	1979	Imperial-Valley	6.5	SS	Brawley Airport	Forward-Dir.	11.3	D	1	225	0.16	35.85	22.39	14.87	0.23
16	1979	Imperial-Valley	6.5	SS	EC Meloland Overpass	Forward-Dir.	3.1	D	1	270	0.30	90.46	31.68	6.75	0.31
17	1983	Coalinga	6.5	TH/REV	Pleasant Valley P. P. Bld.	Forward-Dir.	8.5	–	1	045	0.38	32.40	6.42	8.14	0.09
18	1984	Morgan Hill	6.1	SS	Gilroy STA #2	Forward-Dir.	11.8	D	2	090	0.21	12.75	1.98	12.68	0.06
19	1984	Morgan Hill	6.1	SS	Gilroy STA #3	Forward-Dir.	10.3	D	2	090	0.19	12.23	2.58	22.02	0.06
20	1984	Morgan Hill	6.1	SS	Gilroy STA #6	Forward-Dir.	6.1	C	2	090	0.29	36.54	5.21	6.50	0.13

(*Continued*)

TABLE 1 (*Continued*)

No.	Year	Earthquake	M_w	Mech.[1]	Station	Near Fault Characteristics	Dist.[2] (km)	Site Class[3]	Data Src.[4]	Comp.	PGA (g)	PGV (cm/s)	PGD (cm)	T_D 5 (s)	V/A[6] (s)
21	1984	Morgan Hill	6.1	SS	Coyote Lake Dam	Forward-Dir.	1.5	B	2	285	1.16	80.29	10.53	3.42	0.07
22	1984	Morgan Hill	6.1	SS	Halls Valley	Forward-Dir.	2.5	D	2	240	0.31	39.52	6.56	10.76	0.13
23	1984	Morgan Hill	6.1	SS	Anderson Dam	Forward-Dir.	4.8	B	2	340	0.29	28.00	5.75	5.23	0.10
24	1985	Nahanni-Canada	6.9	–	Site 1, Stn. 6097	Forward-Dir.	6.0	–	1	010	0.98	46.05	9.62	7.90	0.05
25	1986	N. Palm Springs	6.2	SS	Whitewater Trout Farm	Forward-Dir.	6.1	–	1	270	0.61	31.48	4.59	3.41	0.05
26	1986	N. Palm Springs	6.2	SS	Desert Hot	Forward-Dir.	6.8	D	1	000	0.33	29.46	5.70	6.55	0.09
27	1986	N. Palm Springs	6.2	SS	N. Palm Spr. Post Office	Forward-Dir.	3.6	–	1	210	0.59	73.27	11.47	4.58	0.13
28	1987	Superstition Hills	6.4	SS	Parachute Test Site	Forward-Dir.	0.7	D	1	225	0.46	111.99	52.46	10.33	0.25
29	1987	Superstition Hills	6.4	SS	El Centro Imp. Co. Cent.	Forward-Dir.	13.9	D	1	000	0.36	46.36	17.58	32.10	0.13
30	1987	Whittier-Narrows	6.1	TH/REV	LA Vernon Ave., Cmd Terminal	Forward-Dir.	15.7	D	1	083	0.15	13.14	1.43	11.92	0.09
31	1987	Whittier-Narrows	6.1	TH/REV	Bell LA Bulk Mail Center	Forward-Dir.	14.9	B	2	010	0.33	13.90	1.49	7.24	0.04
32	1987	Whittier-Narrows	6.1	TH/REV	Garvey Reservoir Abutment Bld.	Forward-Dir.	13.6	B	2	060	0.37	15.53	1.42	5.69	0.04
33	1989	Loma Prieta	7.0	OB	Gilroy Gav. Col.	Forward-Dir.	11.6	C	1	067	0.36	28.63	6.36	5.00	0.08
34	1989	Loma Prieta	7.0	OB	Los Gatos Parent Center	Forward-Dir.	3.5	C	1	000	0.56	94.81	41.13	10.18	0.17

35	1989	Loma Prieta	7.0	OB	Lexington Dam	Forward-Dir.	6.3	C	2	090	0.41	94.26	36.36	4.12	0.23
36	1989	Loma Prieta	7.0	OB	Gilroy STA #1	Forward-Dir.	2.8	B	1	090	0.47	33.96	8.09	14.72	0.07
37	1989	Loma Prieta	7.0	OB	Gilroy STA #2	Forward-Dir.	4.5	D	1	000	0.37	32.92	7.19	10.98	0.09
38	1989	Loma Prieta	7.0	OB	Gilroy STA #3	Forward-Dir.	6.3	D	1	000	0.56	35.70	8.24	6.37	0.07
39	1989	Loma Prieta	7.0	OB	Gilroy His. Bld.	Forward-Dir.	12.7	–	1	090	0.28	41.97	11.12	8.92	0.15
40	1989	Loma Prieta	7.0	OB	Saratoga Aloha Ave.	Forward-Dir.	4.1	D	2	090	0.32	44.77	27.97	8.26	0.14
41	1989	Loma Prieta	7.0	OB	Saratoga W. Valley Coll.	Forward-Dir.	13.7	–	1	000	0.26	42.45	19.51	11.11	0.17
42	1989	Loma Prieta	7.0	OB	Capitola	Forward-Dir.	8.6	D	1	000	0.53	35.03	9.17	11.92	0.07
43	1989	Loma Prieta	7.0	OB	Corralitos	Forward-Dir.	5.1	D	1	000	0.64	55.20	10.75	6.88	0.09
44	1992	Landers	7.3	SS	Lucerne Valley	Forward-Dir.	2.0	B	1	275	0.72	97.71	70.35	13.12	0.14
45	1992	Landers	7.3	SS	Joshua Tree Fire Stn.	Forward-Dir.	10.0	D	1	000	0.27	27.50	9.12	27.22	0.10
46	1992	Cape Mendocino	7.1	TH	Petrolia, General Store	Forward-Dir.	15.9	C	1	090	0.66	90.16	28.89	16.08	0.14
47	1992	Erzincan	6.7	SS	Erzincan	Forward-Dir.	2.0	C	1	EW	0.50	64.32	21.93	7.35	0.13
48	1994	Northridge	6.7	TH	Rinaldi Rec. Stn.	Forward-Dir.	8.6	D	2	S49W	0.84	174.79	33.40	7.05	0.21
49	1994	Northridge	6.7	TH	Newhall LA Fire Stn.	Forward-Dir.	7.1	D	1	090	0.58	75.63	18.91	5.92	0.13
50	1994	Northridge	6.7	TH	Newhall Pico Canyon	Forward-Dir.	7.1	D	1	316	0.33	67.44	16.11	9.23	0.21
51	1994	Northridge	6.7	TH	Jensen Filt. Plant	Forward-Dir.	6.2	D	1	022	0.42	106.30	43.25	12.40	0.26
52	1994	Northridge	6.7	TH	Sepulveda Va. Hospital	Forward-Dir.	9.5	D	1	360	0.94	75.92	15.10	8.18	0.08
53	1994	Northridge	6.7	TH	Pacoima Kagel Canyon	Forward-Dir.	10.6	B	1	360	0.43	51.57	8.19	9.84	0.12
54	1994	Northridge	6.7	TH	Canoga Park TC	Forward-Dir.	15.7	D	1	196	0.42	60.73	20.30	10.40	0.15
55	1994	Northridge	6.7	TH	Arieta Nordhoff Ave. Fire Stn.	Forward-Dir.	9.5	D	1	090	0.34	40.66	15.07	12.98	0.12

(*Continued*)

TABLE 1 (*Continued*)

No.	Year	Earthquake	M_w	Mech.[1]	Station	Near Fault Characteristics	Dist.[2] (km)	Site Class[3]	Data Src.[4]	Comp.	PGA (g)	PGV (cm/s)	PGD (cm)	T_D 5 (s)	V/A[6] (s)
56	1994	Northridge	6.7	TH	Los Angeles Dam	Forward-Dir.	2.6	–	1	064	0.51	63.70	21.26	6.68	0.13
57	1994	Northridge	6.7	TH	White Oak Covenant Church	Forward-Dir.	12.9	D	2	000	0.33	43.25	9.23	16.74	0.13
58	1994	Northridge	6.7	TH	Sun Valley Roscoe Blvd.	Forward-Dir.	10.5	D	1	000	0.30	22.21	7.86	12.35	0.08
59	1994	Northridge	6.7	TH	Knolls Elementary School	Forward-Dir.	14.3	D	2	000	0.73	52.35	6.63	5.92	0.07
60	1994	Northridge	6.7	TH	Sylmar Olive View Hospital	Forward-Dir.	6.4	D	1	360	0.84	130.37	31.72	5.32	0.16
61	1994	Northridge	6.7	TH	Slymar Converter Sta.	Forward-Dir.	6.2	D	1	142	0.90	102.20	45.11	7.47	0.12
62	1994	Northridge	6.7	TH	Slymar Converter Sta East	Forward-Dir.	6.1	D	1	018	0.83	117.51	34.47	6.90	0.14
63	1995	Koba	6.9	SS	Takatori	Forward-Dir.	4.3	D	1	090	0.62	120.78	32.75	9.93	0.20
64	1995	Koba	6.9	SS	KJMA	Forward-Dir.	0.6	C	1	000	0.82	81.62	17.71	8.36	0.10
65	1999	Kocaeli	7.4	SS	Darica	Fling	17.0	C	3	EW	0.14	45.06	66.09	29.54	0.33
66	1999	Kocaeli	7.4	SS	Duzce	Forward-Dir.	11.0	D	1	180	0.31	58.85	44.10	11.79	0.19
67	1999	Kocaeli	7.4	SS	Gebze	Forward-Dir.	15.0	B	1	000	0.24	50.30	42.69	29.59	0.21
68	1999	Duzce	7.2	SS	Bolu	Forward-Dir.	20.4	D	1	EW	0.82	62.13	13.57	9.03	0.08
69	1999	Chi-Chi	7.6	TH	TCU052	Fling	1.8	D	4	EW	0.35	178.00	493.52	16.80	0.52
70	1999	Chi-Chi	7.6	TH	TCU052	Fling	1.8	D	4	NS	0.44	216.00	709.09	15.93	0.50
71	1999	Chi-Chi	7.6	TH	TCU068	Fling	3.0	D	4	EW	0.50	277.56	715.82	12.37	0.57
72	1999	Chi-Chi	7.6	TH	TCU068	Fling	3.0	D	4	NS	0.36	294.14	895.72	13.24	0.83
73	1999	Chi-Chi	7.6	TH	TCU074	Fling	13.8	D	4	EW	0.59	68.90	193.22	11.82	0.12
74	1999	Chi-Chi	7.6	TH	TCU074	Fling	13.8	D	4	NS	0.37	47.95	155.41	19.71	0.13

75	1999	Chi-Chi	7.6	TH	TCU084	Fling	11.4	C	4	EW	0.98	140.43	204.59	14.65	0.15
76	1999	Chi-Chi	7.6	TH	TCU084	Fling	11.4	C	4	NS	0.42	42.63	64.91	23.14	0.10
77	1999	Chi-Chi	7.6	TH	TCU129	Fling	2.2	D	4	EW	0.98	66.92	126.13	27.35	0.07
78	1999	Chi-Chi	7.6	TH	TCU129	Fling	2.2	D	4	NS	0.61	54.56	82.70	30.79	0.09
79	1999	Kocaeli	7.4	SS	Yarimca	Fling	3.3	D	3	EW	0.23	88.83	184.84	33.16	0.39
80	1999	Kocaeli	7.4	SS	Yarimca	Fling	3.3	D	3	NS	0.33	88.38	152.12	31.84	0.27
81	1999	Kocaeli	7.4	SS	Izmit	Fling	4.3	B	3	NS	0.17	27.19	23.67	34.07	0.16
82	1999	Kocaeli	7.4	SS	Izmit	Fling	4.3	B	3	EW	0.23	48.87	95.49	34.49	0.22
83	1999	Kocaeli	7.4	SS	Sakarya	Fling	3.2	C	3	EW	0.41	82.05	205.93	14.63	0.20
84	1999	Chi-Chi	7.6	TH	TCU102	Fling	1.2	D	4	NS	0.17	68.62	83.78	19.74	0.41
85	1999	Chi-Chi	7.6	TH	TCU102	Fling	1.2	D	4	EW	0.29	84.52	153.88	14.98	0.30
86	1999	Chi-Chi	7.6	TH	TCU089	Fling	8.3	C	4	NS	0.22	33.92	141.33	24.87	0.16
87	1999	Chi-Chi	7.6	TH	TCU089	Fling	8.3	C	4	EW	0.34	44.43	193.90	24.12	0.13
88	1999	Chi-Chi	7.6	TH	TCU049	Fling	3.3	D	4	NS	0.24	57.49	102.66	22.70	0.24
89	1999	Chi-Chi	7.6	TH	TCU049	Fling	3.3	D	4	EW	0.27	54.79	121.77	21.64	0.21
90	1999	Chi-Chi	7.6	TH	TCU067	Fling	1.1	D	4	NS	0.31	53.47	103.20	22.99	0.18
91	1999	Chi-Chi	7.6	TH	TCU067	Fling	1.1	D	4	EW	0.48	94.31	181.25	21.71	0.20
92	1999	Chi-Chi	7.6	TH	TCU075	Fling	3.4	D	4	NS	0.25	36.17	108.54	31.21	0.15
93	1999	Chi-Chi	7.6	TH	TCU075	Fling	3.4	D	4	EW	0.32	111.79	164.36	27.04	0.36
94	1999	Chi-Chi	7.6	TH	TCU076	Fling	3.2	D	4	NS	0.41	61.76	73.06	28.14	0.15
95	1999	Chi-Chi	7.6	TH	TCU076	Fling	3.2	D	4	EW	0.33	65.93	101.65	29.66	0.20
96	1999	Chi-Chi	7.6	TH	TCU072	Fling	7.9	D	4	NS	0.36	66.73	245.30	24.00	0.19
97	1999	Chi-Chi	7.6	TH	TCU072	Fling	7.9	D	4	EW	0.46	83.60	209.67	21.92	0.19
98	1999	Chi-Chi	7.6	TH	TCU065	Fling	2.5	D	4	NS	0.55	86.37	124.68	28.54	0.16
99	1999	Chi-Chi	7.6	TH	TCU065	Fling	2.5	D	4	EW	0.76	128.32	228.41	28.78	0.17
100	1999	Chi-Chi	7.6	TH	TCU079	Fling	11.0	D	4	NS	0.41	30.41	83.05	26.88	0.08
101	1999	Chi-Chi	7.6	TH	TCU079	Fling	11.0	D	4	EW	0.57	68.06	166.10	24.24	0.12
102	1999	Chi-Chi	7.6	TH	TCU078	Fling	8.3	D	4	NS	0.30	30.89	106.67	26.06	0.10
103	1999	Chi-Chi	7.6	TH	TCU078	Fling	8.3	D	4	EW	0.43	41.88	121.23	25.92	0.10

(*Continued*)

TABLE 1 (*Continued*)

No.	Year	Earthquake	M_w	Mech.[1]	Station	Near Fault Characteristics	Dist.[2] (km)	Site Class[3]	Data Src.[4]	Comp.	PGA (g)	PGV (cm/s)	PGD (cm)	T_D 5 (s)	V/A[6] (s)
104	1999	Chi-Chi	7.6	TH	TCU082	Fling	4.5	D	4	NS	0.18	38.77	105.74	27.02	0.22
105	1999	Chi-Chi	7.6	TH	TCU082	Fling	4.5	D	4	EW	0.22	50.49	142.78	23.26	0.23
106	1999	Chi-Chi	7.6	TH	TCU128	Fling	9.1	C	4	NS	0.16	59.74	88.13	20.66	0.38
107	1999	Chi-Chi	7.6	TH	TCU128	Fling	9.1	C	4	EW	0.14	59.42	91.05	19.26	0.43
108	1999	Chi-Chi	7.6	TH	TCU071	Fling	4.9	D	4	NS	0.63	79.11	244.05	23.74	0.13
109	1999	Chi-Chi	7.6	TH	TCU071	Fling	4.9	D	4	EW	0.51	69.91	196.85	24.60	0.14
110	2004	Bingol	6.4	SS	Bingol	Forward-Dir.	6.1	D	3	NS	0.56	14.65	9.82	4.5t9	0.03
111	2004	Parkfield	6.4	SS	Cholame 1E	Forward-Dir.	6.5	D	5	FN	0.47	53.10	12.83	4.96	0.12
112	2004	Parkfield	6.4	SS	Cholame 5W (Sta 5)	Forward-Dir.	10.0	D	5	FN	0.21	17.38	2.41	22.14	0.08
113	2004	Parkfield	6.4	SS	Fault Zone 1	Forward-Dir.	3.4	D	5	FN	0.50	64.15	12.64	8.90	0.13
114	2004	Parkfield	6.4	SS	Gold Hill 1W	Forward-Dir.	0.8	D	5	FN	0.13	6.98	2.01	15.34	0.05

[1]Faulting Mechanism = TH: Thrust; REV: Reverse; SS: Strike-slip; OB: Oblique.
[2]Closest distance to fault rupture (i.e., r_{jb}).
[3]NEHRP Site Classifications = > (B for V_S – 760 to 1500 m/s), (C for V_S = 360 to 760 m/s), (D for V_S = 180 to 360 m/s).
[4]Data Source = 1: PEER (http://peer.herkeley.edu/smcat); 2: Cosmos (http://db.cosmos-eq.org); 3: ERD (http://angora.deprem.gov.ir/); 4: http://scman.cwb.gov.tw/eqv5/special/19990921/pgadata-asc10704.htm 5: CSMIP (http://www.quake.ca.gov/cisn-edc/idr/Parkfield_28Sep2004/idr_dist.htm).
[5]T_D = Duration of motion (time interval during which accelerogram Arias intensity increases from 5–95% of its final value).
[6]V/A - PGV/PGA (Indicates the average duration of acceleration pulse provided that PGV is reached immediately following the dominant acceleration pulse).
Note: Original fling ground motions from data sources (3) and (4) were baseline corrected after removal of pre-event mean (For details see Kalkan and Kummath, 2006a).

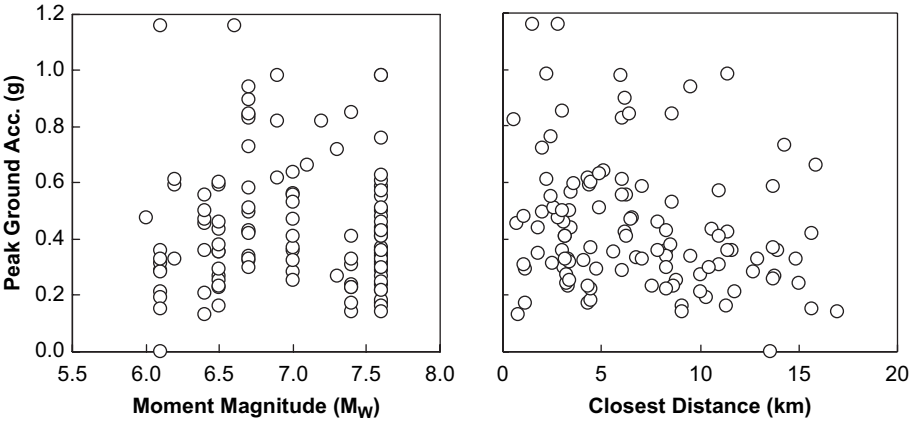

FIGURE 3 Distribution of PGA of records with respect to moment magnitude (left) and closest fault distance (right).

$$E_K^{'} + E_D + E_H = E_I^{'} \tag{2}$$

where $E_K^{'}$ is the relative kinetic energy, E_D is the damping energy, E_H is the hysteretic energy composed of elastic strain energy (E_S) and plastic strain energy (E_P) (i.e., irrecoverable hysteretic energy). It is possible to expand Eq. 2 into its respective components:

$$\frac{m(\dot{u})^2}{2} + \int c\dot{u}du + \int f(u)du = -\int m\ddot{u}_g du = -\int m\ddot{u}_g \dot{u}dt \tag{3}$$

in which m is the mass, c is the damping coefficient, $f(u)$ is the restoring force, u is the relative displacement of the SDOF oscillator with respect to the ground, and $\ddot{u}_g$ is the ground acceleration. Note that $\ddot{u}$ and $\dot{u}$ are time-derivatives of u (i.e., $du = \dot{u}dt$). Hence, Eq. 3 can be easily integrated in the time-domain.

Energy is generally represented as the energy equivalent velocity ($V_{eq} = \sqrt{2E_I^{'}/m}$) since this term is linearly proportional to the ground motion amplitude. For convenience, V_{eq} is henceforth referred to as input energy. The responses shown in Figure 4 provide an opportunity to assess the variation of seismic demand and its correlation to different components of input energy.

Owing to the fact that damage to a structural component is directly related to dissipated energy, Figure 4 demonstrates the combined effects of damping and hysteretic energy (E_H + E_D) separately in addition to the relative input energy ($E_I^{'}$) and damping energy (E_D). The plots showing the energy components indicate that the kinetic energy component vanishes during reversal of system velocity (i.e., $\dot{u}(t) = 0$ at the point of zero crossings in the velocity time-response), and the summation of damping and hysteretic energy becomes equal to the relative input energy. These time instants ($\dot{u}(t) = 0$) also refer to the corner points in the force-deformation hysteresis loops representing the absolute peak displacements during each cycle. The energy balance equation between these two peaks in the displacement response can be expressed as

$$\Delta E_D + \Delta E_H = \Delta E_I \tag{4}$$

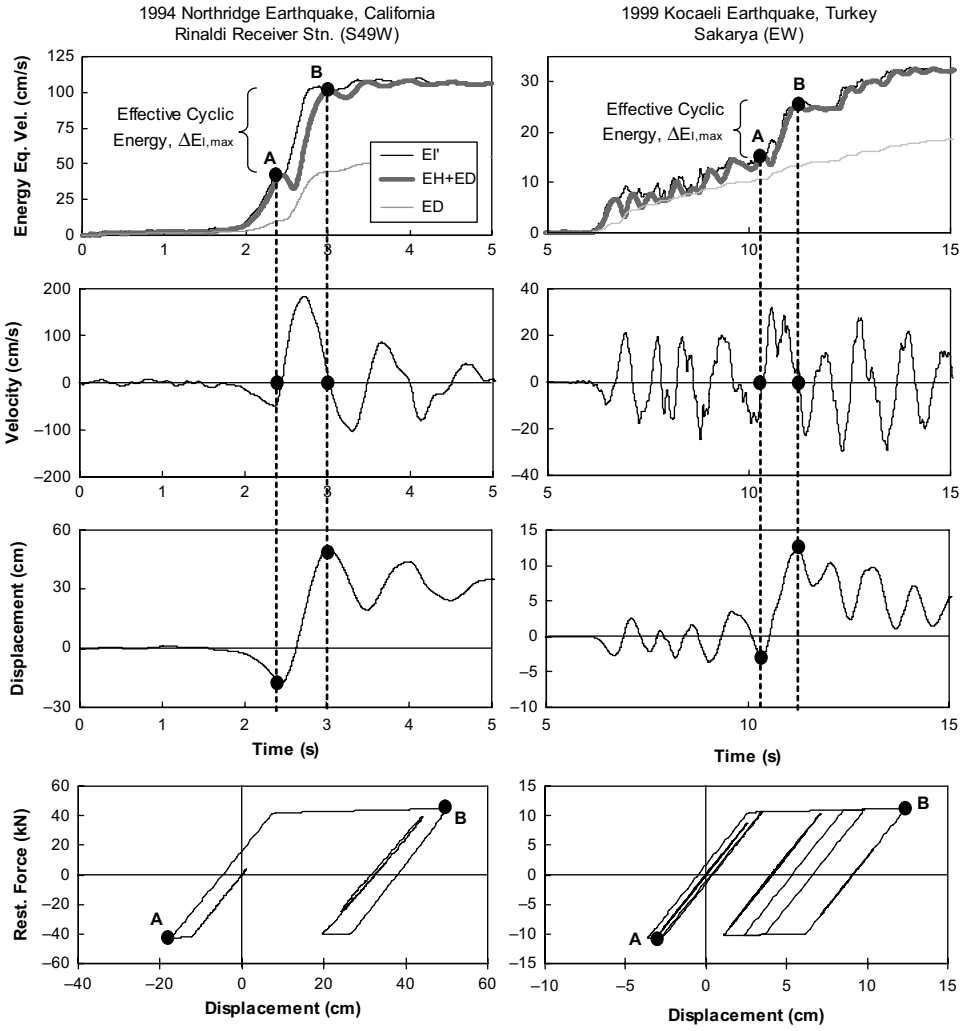

FIGURE 4 Correlation of SDOF oscillator inelastic response with computed ECE for near-fault forward directivity record of Rinaldi Rec. Stn. and fling record of Sakarya ($T_{elastic}$ = 1.0s, μ = 4.0).

where ΔE_D is the incremental energy due to viscous damping, and ΔE_H includes both the incremental recoverable strain energy (ΔE_S) and irrecoverable strain energy (ΔE_P). The peak value of the term on the right-hand side of the Eq. 4 (i.e., $\Delta E_{I,\max}$) is hereby defined as the ECE. The definition of ECE represents the incremental work done during the finite time interval ($\Delta t = t_2 - t_1$) between two zero-crossings of the effective system velocity (i.e., $\dot{u}(t_2) = 0$ and $\dot{u}(t_1) = 0$). As shown in Figure 4, ECE attains its largest magnitude immediately before the maximum displacement. Similar observations were noted for the all the impulsive records (i.e., records exhibiting a predominant pulse) considered in the study [Kalkan, 2006]. It is also noteworthy that ECE depends not only on the ground motion characteristics but also on the system attributes (such as period, hysteretic rule, damping, ductility, etc.). Although Eqs. 2 and 3 are derived for relative input energy, ECE (see Eq. 4) is not affected by the choice of absolute or relative energy since the difference in

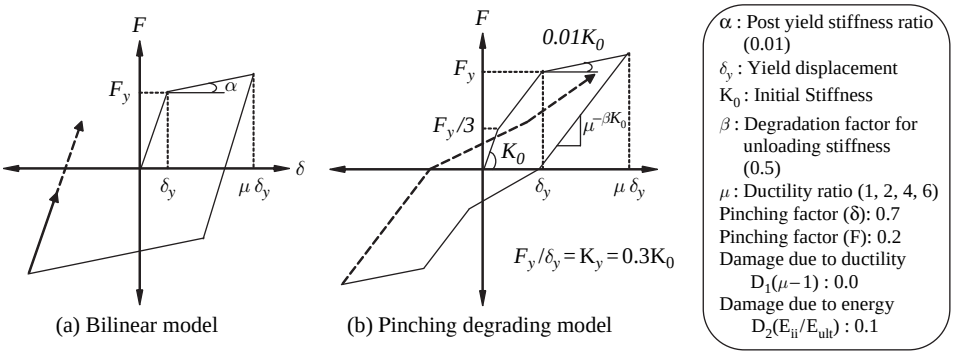

FIGURE 5 Hysteretic models.

the two energy definitions in fact arises from the formulation of the kinetic energy term (Eq. 1), which vanishes in the ECE formulation.

4. ECE-Based Ground Motion Severity Index

The concept of energy balance has been extensively used to identify reliable relationships between seismic energy and displacement demands, and consequently develop indices to effectively capture the destructive potential of earthquake motions. Fajfar [1992] derived the following non dimensional parameter based on the reduction of the deformation capacity due to low-cycle fatigue.

$$\gamma = \frac{\sqrt{E_H / m}}{\omega D} \tag{5}$$

where E_H represents the dissipated hysteretic energy, m is the mass of the system, ω is the natural frequency, and D is the maximum displacement demand. This index, which is the ratio of two equivalent velocities, has been shown to be dependent on both ground motion and system attributes but independent of damping [Fajfar and Vidic, 1994]. An analogous parameter (ζ) was later proposed by Teran-Gilmore [1998] whereby the hysteretic energy term (E_H) in Eq. 5 was replaced with the absolute input energy term (E_I) as in the following:

$$\zeta = \frac{\sqrt{E_I / m}}{\omega D}. \tag{6}$$

This parameter is shown to be more stable than γ [Teran-Gilmore, 1998; Decanini *et al.*, 2001]. Other response indices correlating the maximum displacement demand to seismic energy utilizes the ratio of hysteretic energy to total input energy (i.e., absolute energy) (E_H/E_I) as used in studies by Kuwamura and Galambos [1989], Fajfar and Vidic [1994], Lawson and Krawinkler [1995], and Decanini and Mollaioli [2001] and the square root of hysteretic energy $S_H = \sqrt{E_H}$ proposed by Riddell and Garcia [2001].

Following a detailed and comprehensive study examining peak response measures and seismic energy (Figure 4 being a representative set) of SDOF systems, it was

established that ECE (i.e., $\Delta E_{I,\,\max}$) is a reliable measure of the critical seismic energy transferred to a structural system and producing the maximum cyclic deformation in a single effective cycle. On the basis of this finding, the hysteretic energy term in Eq. 5 was replaced with ECE resulting in an alternative descriptor, denoted by γ_{eff} as follows:

$$\gamma_{eff} = \frac{\sqrt{(\Delta E_{I,\max})/m}}{\omega D}. \tag{7}$$

The stability and accuracy of this new descriptor is investigated for 114 near-fault recordings. Pertinent information on the ground motion data is listed in Table 1, Table 1 also includes data on the ratio of PGA to PGV (denoted as *V/A*) and strong motion duration (T_D) of the recordings. *V/A* ratio indicates the average duration of the acceleration pulse provided that the PGV is reached immediately following the dominant acceleration pulse. This parameter has been shown to correlate well with the damage potential [Sucuoglu *et al*., 1998] and peak input energy of recordings [Kalkan, 2006]. Strong motion duration (T_D) is another parameter used commonly to identify the severity of ground motions [e.g., Uang and Bertero, 1990; Amiri and Dana, 2005]. It was first defined by Trifunac and Brady [1975] as the interval between times at which 5 and 95% of the value of the Arias intensity ($I_A = (\pi/2g)\int_0^{t_d} \ddot{u}_g^2 dt$, where t_d is the duration of record) is achieved.

Using the ground motion records listed in Table 1, the correlation between peak seismic demand and the proposed energy (ECE) and damage (γ_{eff}) measures is evaluated and also compared to other indices. The analyses considered two different hysteretic models at four different ductility levels (μ = 1, 2, 4, and 6). A bilinear non degrading hysteretic model and a pinched-degrading model were employed in the inelastic SDOF time-history analyses. The numerical simulations were carried out using an open-source finite element platform [Opensees, 2006]. The hysteretic models utilized are one of the available uniaxial material models called "hysteretic" model. Figure 5 shows the parameters used to define the model. For the pinched-degrading model, the degradation of material parameters is based on a damage function that depends on weighted sum of normalized plastic energy dissipation (i.e., damage due to energy) and deformation ductility (i.e., damage due to ductility), while pinching is included by defining a lower intermediate level of yielding and corresponding post-yield (pinching) stiffness. The material coefficients given in Figure 5 were selected to have reasonably moderate pinching and degrading effects. Further details of the cyclic degrading model used can be found in Spacone *et al.* [1992].

Figures 6 and 7 summarize the correlation between peak system displacement and effective cyclic energy (ECE), absolute input energy (E_I), peak elastic displacement ($\delta_{\max,e}$), and *V/A* ratio computed based on two force-deformation models for short (T = 0.5s) and long period (T = 3.0s) systems with a ductility ratio of 6. These plots indicate that ECE is better correlated to peak system deformation than parameters such as E_I, $\delta_{\max,e}$, or *V/A*. Both relative and absolute input energy comparisons produced similar results, and general findings from these two figures are valid also for the period range of 0.1–5.0 s and ductility ratios of 1, 2, 4, and 6. In contrast to ECE, the poorest correlation was observed between strong motion duration (T_D) and peak system deformation and therefore not included in Figures 6 and 7. This finding is not surprising since it is well-know that strong motion duration is not significant for near-fault records. On the other hand, *V/A* ratios are better correlated with peak deformation particularly for long period systems. For short period systems, its correlation is again poor. The performance of $\delta_{\max,e}$ to predict maximum deformation demand is comparable with E_I in the case of the bilinear model, while it

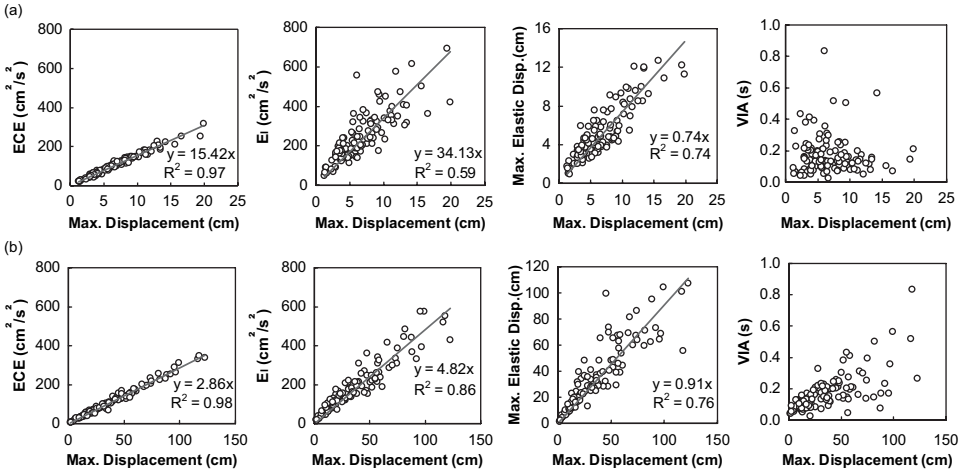

FIGURE 6 Correlation between peak inelastic system displacement and ECE, absolute input energy (E_I), elastic peak displacement ($\delta_{max,e}$), and ratio of PGA to PGV (V/A) computed for bilinear hysteretic model having constant displacement ductility ratio of 6 at (a) T = 0.5 s and (b) T = 3.0 s.

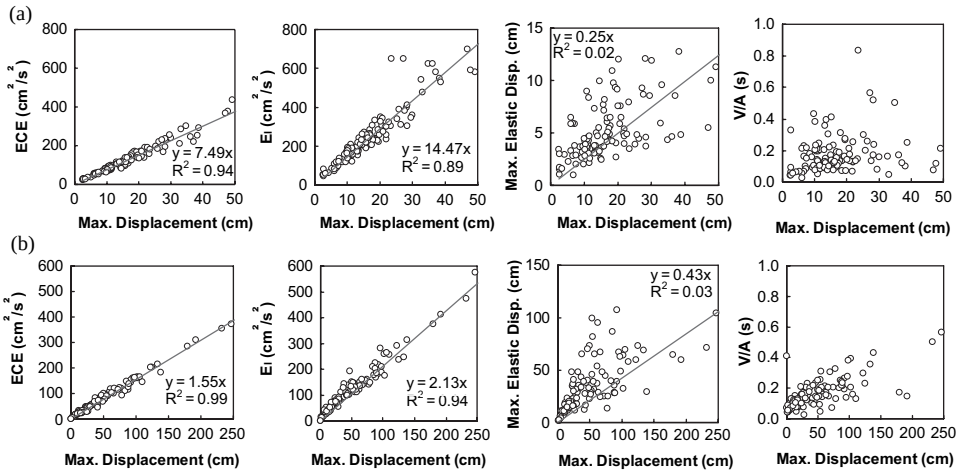

FIGURE 7 Correlation between maximum system displacement and ECE, absolute input energy (E_I), elastic peak displacement ($\delta_{max,e}$), and ratio of PGA to PGV (V/A) computed for pinched-degrading hysteretic model having constant displacement ductility ratio of 6 at (a) T = 0.5s and (b) T = 3.0s.

shows larger scatter in the case of the pinched-degrading model. This observation on $\delta_{\max,e}$ is consistent with previous studies reported by Ramirez *et al.* [2002], Ruiz-Garcia and Miranda [2003] and Chopra and Chintanapakdee [2003]. In fact, $\delta_{\max,e}$ is a common response predictor and widely used to estimate target displacement in nonlinear static procedures (FEMA-356, 440). Yet, as shown, its ability to predict deformation demand is inadequate as the inelasticity in the system increases. Owing to this fact, the FEMA

displacement coefficient method [ATC 2005] requires amplification on $\delta_{max,e}$ through *C1* (maximum displacement ratio) and *C2* (adjustment for cyclic degradation) coefficients based on elastic period (*T*) and response modification factor (R).

It should be also noted that the peak displacement values of SDOF systems were computed in constant ductility space. For different hysteretic models, to satisfy the constant ductility ratio, yield strength (f_y) was varied for each spectral period. Even for the same elastic period, bilinear hysteretic and pinched-degrading hysteretic models provide different yield strengths, hence the peak displacement demands of the two models differ. In lieu of constant-ductility space, if the constant-R [$R = f_{max}/f_y$ where $f_{max} = mSa(T)$] space had been utilized, yield strength of both hysteretic models would then be identical and peak displacement values obtained from different hysteretic models would be closer to each other [Gupta and Kunnath, 1998].

It is also noteworthy that the constant slope of the best-fit line in Figures 6 and 7 is directly related to the non dimensional parameter γ_{eff} (see Eq. 7). To further evaluate the accuracy and stability of γ_{eff}, it is compared in Figures 8 and 9 with other non dimensional response indices, namely γ, ζ, and E_H/E_I considering two force-deformation models. Despite some dispersion at small deformations, γ_{eff} generally yields more stable results than other indices. None of the existing measures of damage potential (i.e., γ, ζ, and E_H/E_I) is seen to provide consistent estimates. Therefore, Figures 6–9 collectively indicate that ECE and its counterpart γ_{eff} are stable and reliable indicators of input energy and damage potential of ground shaking. Hence, the energy dissipated through inelastic deformations in an effective cycle (i.e., through damping and dissipated hysteretic energy) is a critical parameter that is most closely correlated with the peak system response for near-fault impulsive ground motions. This suggests the feasibility of determining the maximum seismic demand from the effective cyclic energy.

5. Effective Cyclic Energy Demands in MDOF Systems

Absolute energy formulation for MDOF systems was initially derived by Uang and Bertero [1990]. In a similar manner, it is possible to express the relative energy imparted to a MDOF system as:

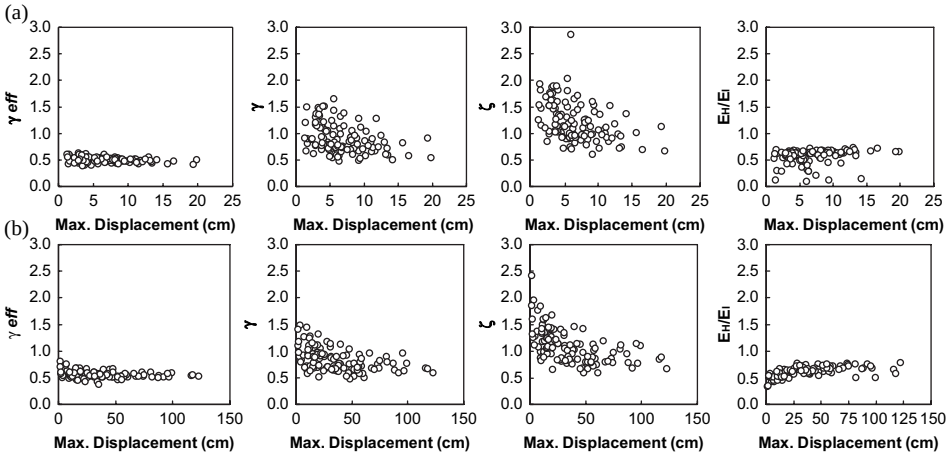

FIGURE 8 Variability of various non-dimensional response indices computed for bilinear hysteretic model having constant displacement ductility ratio of 6 at (a) T = 0.5s and (b) T = 3.0s.

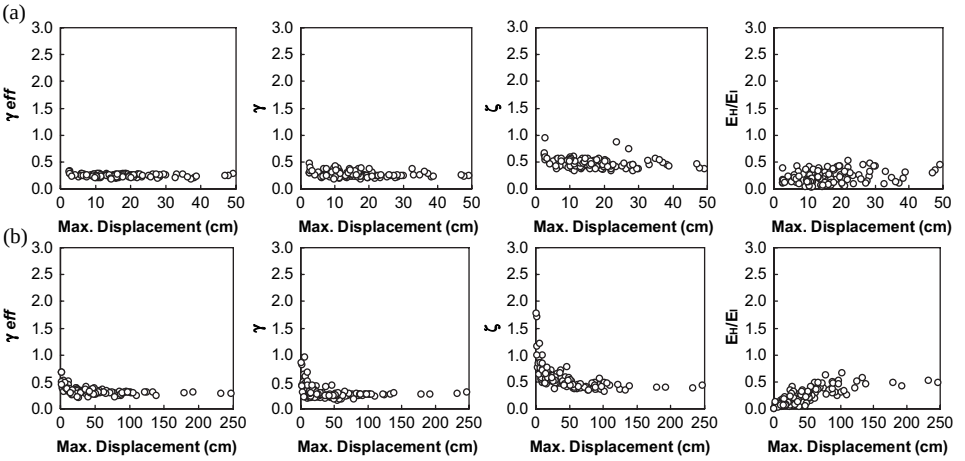

FIGURE 9 Variability of various non-dimensional response indices computed for pinched-degrading hysteretic model having constant displacement ductility ratio of 6 at (a) T = 0.5s and (b) T = 3.0s.

$$\frac{1}{2}\dot{u}^T \boldsymbol{m}\dot{u} + \int \dot{u}\boldsymbol{c}d\boldsymbol{u} + \int f_s \, d\boldsymbol{u} = -\int \boldsymbol{m}\ddot{u}_g d\boldsymbol{u} = -\int \left(\sum_{j=1}^{N} m_j \ddot{u}_g \dot{u}_j\right) dt \tag{8}$$

$$E_K + E_D + (E_S + E_P) = E_I' \tag{9}$$

where $\boldsymbol{m}$ is the diagonal mass matrix, $\boldsymbol{c}$ is the damping matrix, and $\boldsymbol{u}$ is the relative story displacement vector. Accordingly, m_j is the lumped mass and $\dot{u}_j$ is the relative velocity recorded at the j^{th} story, and N is the number of stories. In the above expression, E_I corresponds to the relative work done due to the sum of inertia forces ($m_j\ddot{u}_g$) at each story level over the corresponding story displacement u_j. Chou and Uang [2003] showed that the hysteretic energy component of MDOF systems (i.e., $E_S + E_P$) can be predicted using equivalent-single-degree-of-freedom (ESDOF) systems derived from the first and second mode elastic modal properties. Based on this approach, relative input energy time-history is computed for a MDOF system and compared with the corresponding input energy of ESDOF systems. The MDOF system studied for this purpose is an existing six-story steel moment-frame building instrumented by the California Strong Motion Instrumentation Program. Recorded acceleration time-series at different story levels were initially used in calibration of the numerical model. Details of the modeling and calibrations can be found in Kunnath *et al*. [2004] and Kalkan [2006]. The six-story building has elastic modal periods of 1.41, 0.51, and 0.30 s and modal participation factors of 2.57, 0.96, and 0.47 for the first, second, and third mode, respectively. These properties are used to obtain corresponding ESDOF systems parameters through individual pushover analyses conducted using invariant load vectors. The load vectors correspond to height-wise distribution of inertial forces expressed as $s_n = \Phi_n.\mathbf{m}$ (where Φ_n is the elastic nth-mode vector). In order to approximate the ESDOF parameters through equivalent bi-linearization, spectral conversion of base-shear (i.e., spectral acceleration) is achieved using a procedure similar to ATC-40 [1996], whereas spectral displacement is computed by dividing the total dissipated

energy during the monotonic pushover analysis to the corresponding base shear during each displacement increment. Thereby the ESDOF system is forced to dissipate the same energy dissipated by the MDOF system at each step of the pushover analysis. In this way, potential limitations and drawbacks of using the roof displacement as a deformation index to convert the MDOF capacity curve to the ESDOF system capacity spectrum for modes higher than first mode are eliminated. It is instructive to note that proportionality of the roof displacement to the other story displacements is only limited to the first mode. The energy-based approach for ESDOF conversion of MDOF system has been recently developed in Hernandez-Montes *et al*. [2005] and extended to be used in the adaptive multimodal pushover analysis procedure proposed by Kalkan and Kunnath [2006b].

Figure 10a displays the relative input energy time-variation computed through Eq. 8 for the MDOF system subjected to near-fault forward-directivity record of 1992 Erzincan (Turkey) Earthquake. This record contains a coherent long period velocity pulse associated with distinct pulse content in the acceleration time-series. The record is scaled by 2.0 to create significant inelastic demands, hence the peak inter-story drift ratio (IDR = relative displacement between two consecutive stories normalized by story height) exceeds 3% and significant yielding takes place throughout the structure. Note that first yielding initiates at the first-story column when the peak IDR reaches 0.8% at that story. Also

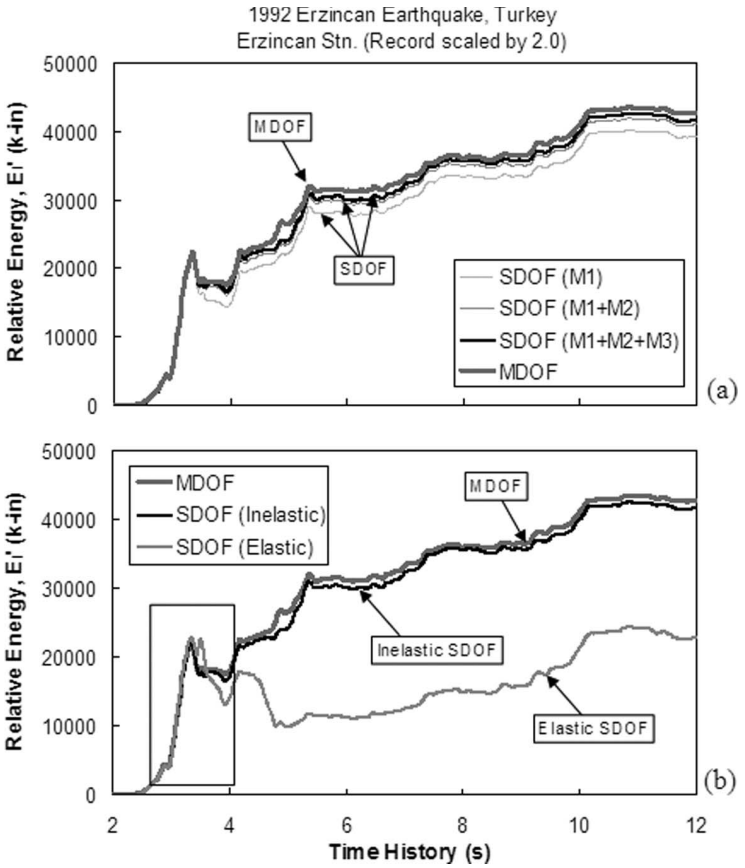

FIGURE 10 Comparison of relative input energy (M1 = Mode 1; M2 = Mode 2; M3 = Mode 3).

shown in Figure 10a are the relative input energy plots computed from the ESDOF systems for comparison. Relative input energy of each ESDOF system ($E'_{I(ESDOF),n}$) is calculated through inelastic time-history analysis and converted to the MDOF n^{th}-mode input energy contribution as

$$E'_{I(MDOF),n} = E'_{I(ESDOF),n}\Gamma_n^2 \tag{10}$$

where Γ_n is the modal participation factor for the n^{th} mode considered. Figure 10a shows that the energy input to MDOF system can be estimated by summation of the energies of the first few modes (generally up to two or three). Thus, the relative input energy to MDOF system can be approximated as:

$$E'_{I(MDOF)} = \sum_{n=1,3} E'_{I(ESDOF),n}\Gamma_n^2. \tag{11}$$

The right-hand side of the Eq. 10 can be interpreted as a "modal-energy-decomposition" approach. Figure 10b compares the input energy computed from the elastic SDOF with the inelastic SDOF time-history analyses (for modes 1–3) and also the input energy computed using Eq. 8 from nonlinear-time-history (NTH) analysis of the MDOF system. This figure implies that the abrupt intense energy jump, condensed in a short period of time (see window in Figure 10b) which is a characteristic of near-fault pulse-type records, can be reasonably estimated by elastic analyses. The sum of hysteretic and damping components of this abrupt energy increase (i.e., ECE) is directly associated with the peak displacement demand since it is generally dissipated in a single effective cycle. It is also clear that, following the immediate energy input, the elastic and inelastic energy curves start to deviate from each other, and the difference between them becomes the accumulated energy dissipated through plastic excursions.

It is possible to express the sum of hysteretic and damping energies as the difference between input and kinetic energies since the computation of input and kinetic energies for MDOF systems is more convenient than the computation of hysteretic and damping energies. If the relative energy is used, the following expression can be utilized to compute the sum of hysteretic and damping energy terms:

$$\Delta E_I = E_\xi - E_H = E'_I - E_K = \int\Big(\sum_{j=1}^{N} m_j \ddot{u}_g\Big)\dot{u}_j dt - \frac{1}{2}\sum_{j=1}^{N} m_j(\dot{u}_j)^2. \tag{12}$$

Similar to SDOF systems investigated earlier, the ECE (i.e., $\Delta E_{I,\max}$) for MDOF system is equal to the peak incremental value of the sum of viscous damping and hysteretic energies between a peak-to-peak half cycle (see Figure 4). Figure 11a shows the time-history of relative input energy and exemplifies the computation of ECE for a MDOF system. Figure 11b-c shows the interstory drift ratio vs. time variation for selected stories based on the peak IDR profile presented in Figure 11d. The IDR is selected as a representative response parameter since it is well-correlated with component deformations at that story [Kunnath and Kalkan, 2004]. It is useful to note that peak IDR for each story is associated with the ECE. To be more specific, the ECE is dissipated throughout the structure within a single effective cycle resulting in the structural peak responses. As aforementioned, this is

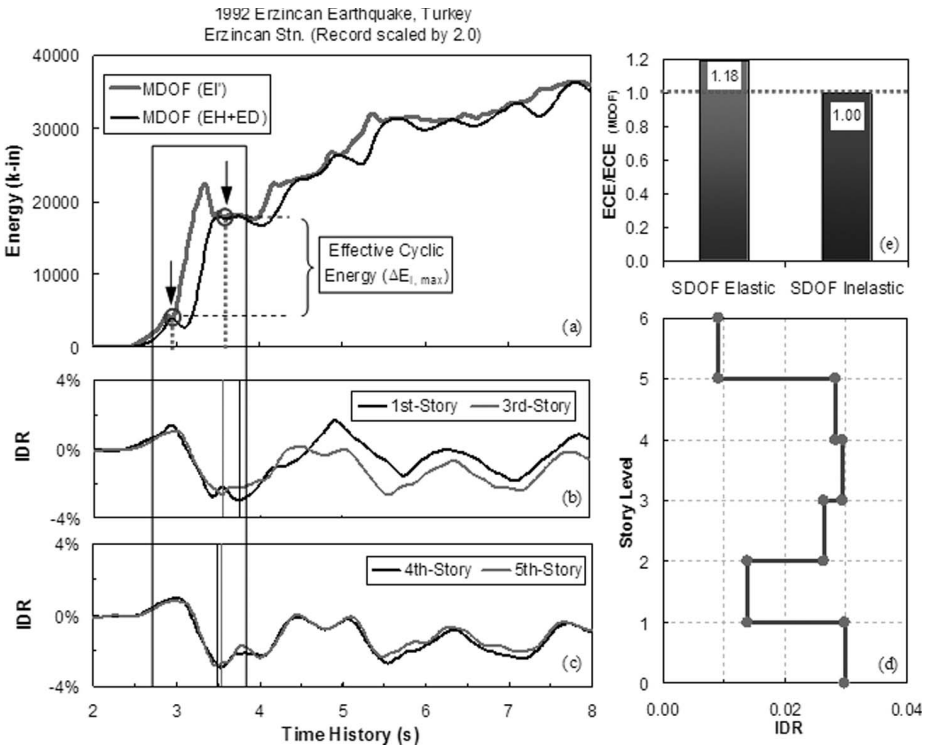

FIGURE 11 Variation of input energy and interstory drift ratio (IDR) for 6-story building and peak interstory drift profile. (Note: time instants for story peak IDR are indicated by vertical lines within the window in Figures 11b–c).

typical for structures subjected to impulsive records. Based on the information gained from Figures 10 and 11 and similar findings for the remaining records in the database, it is concluded that peak inelastic response parameters for pulse-type near-fault earthquakes most possibly take place after the first change of state from elastic to inelastic behavior. Under these conditions, elastic SDOF systems may be potentially used to approximate the ECE input to the MDOF system (see Figure 10b). Figure 11e compares the ECE computed based on the elastic and inelastic ESDOF systems with that of the MDOF system. In generating the ECE, energy contributions of ESDOF systems for the first two modes are summed since energy contribution of the third mode is significantly lower. As seen in this figure the ECE input to MDOF system can be best estimated using inelastic ESDOF systems, yet elastic ESDOF systems can still be utilized for practical purposes since it provides reasonable predictions of ECE demand without requiring priori knowledge on the modal ductility demands.

The good correlation obtained between the ECE of MDOF and SDOF systems allows ECE to be used directly in a spectral format. Figure 12 demonstrates the mean ECE spectra derived for near-fault accelerograms having forward-directivity and fling. It is clear that the ductility ratio has only a marginal effect on the energy demand while the force-deformation modeling can have a more significant impact on the spectral shape. The pinched-degrading model shows tendency to shift the ECE peaks to the lower periods compared to the stable bilinear hysteretic model (ECE spectra of individual records lead to the same conclusion). These plots should again be interpreted in the constant-ductility

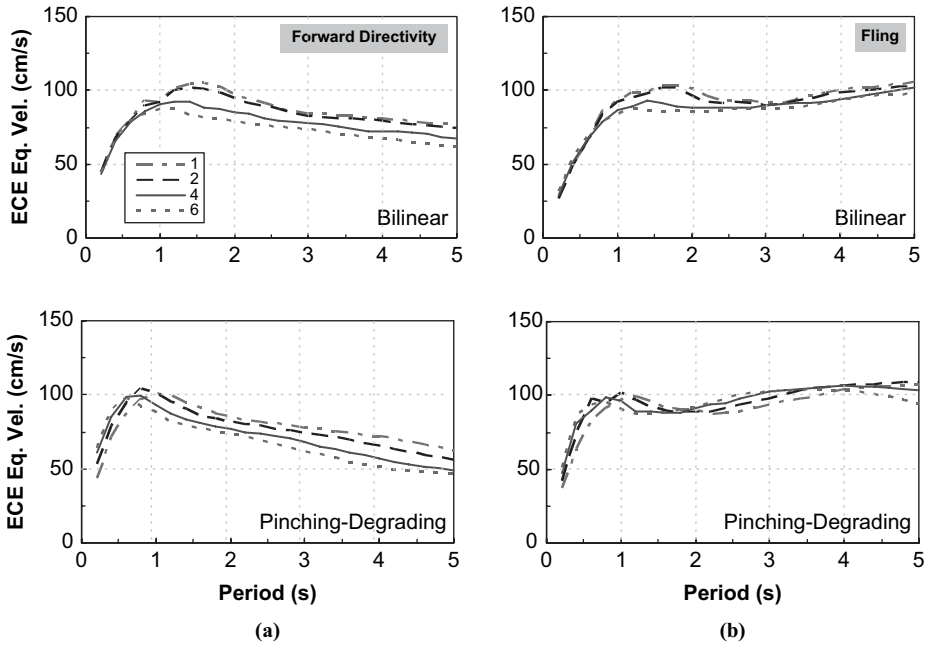

FIGURE 12 Mean ECE equivalent velocity spectra of (a) near-fault forward directivity and (b) fling records in Table 1 computed for two different hysteretic models.

space as aforementioned earlier. ECE spectral shapes are in general similar to acceleration response spectra in a way that they show significant record-to-record variability.

6. Effective Cyclic Energy Demand Estimation

ECE demands of a MDOF system is estimated based on the modal-energy-decomposition (see Eq. 11) and the elastic ECE spectrum. The six-story building described earlier is used to illustrate the proposed concept. Two near-fault records are first employed in the nonlinear time-history simulations to obtain the corresponding performance as well as the ECE of the MDOF system. Figure 13b compares the ECE demand of MDOF system during the nonlinear time history analyses with demands computed based on both inelastic SDOF time history analyses and those computed from the elastic ECE spectra as also illustrated in Figure 13a. The results of inelastic SDOF time-response analyses yield the best estimates since they are more consistent with the modal ductility demands of the MDOF system. However, it is seen that the elastic ECE spectrum provides reasonable predictions. This later approach requires generation of elastic ECE spectrum and limited knowledge on the basic structural characteristics of the MDOF system (i.e., period, damping and participation factor of first few elastic modes).

The modal ECE demands computed using the ECE spectrum (i.e., vertical lines in the ECE plots shown in Figure 13a correspond to T_1 and T_2) are also in good agreement with the peak interstory drift profiles shown in Figure 13c. Results of NTH analyses show that higher mode contributions (i.e., amplified deformations at upper or intermediate stories) to the response are significant in case of TCU068 record, whereas the Parachute Test Site record triggers a primarily first mode response and imposes the largest interstory drift exceeding 4.0% at the first story level. Correlation of the MDOF responses with the ECE

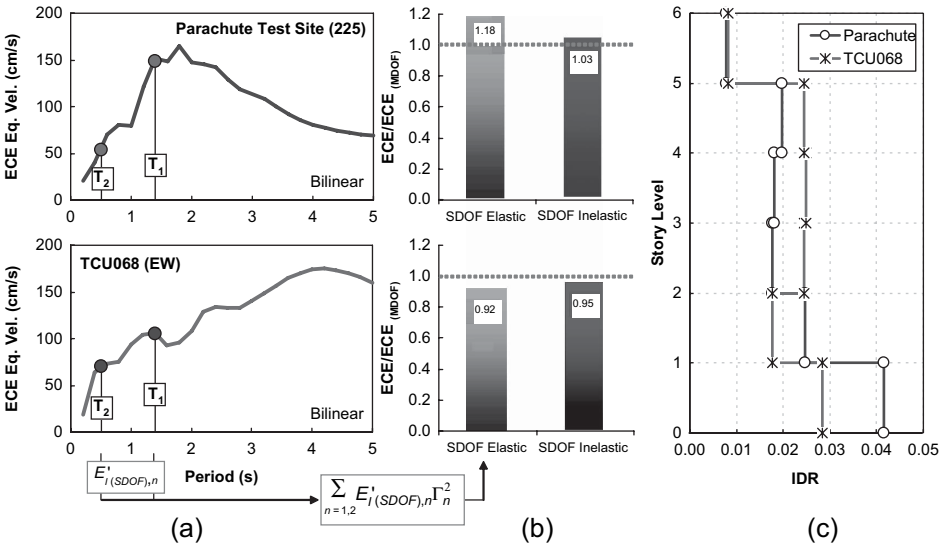

FIGURE 13 ECE demand estimates in MDOF system.

spectrum indicates that the Parachute Test Site record has a significantly larger modal energy demand in the ECE spectrum close to the first mode period of the building than at the higher modes. For the TCU068 record, the ECE spectrum points the likelihood of higher mode participation by providing relatively less energy difference between the first two modes. Moreover, it is evident that the ECE spectra of the records confirm the information gained from the inelastic response of the buildings suggesting the potential of the proposed ECE spectra to distinguish seismic damage potential of ground motion records.

As demonstrated for two cases in Figure 13, it seems possible to estimate the ECE demand of MDOF system using elastic ECE spectrum through modal energy decomposition. Further validation of this approach is performed using 30 pulse-type near-fault records and inelastic MDOF time-history analyses. Table 2 lists these records while their details can be found in Table 1. Figure 14 plots the height-wise statistical distribution of primary response parameters including IDR, roof drift ratio (maximum roof displacement normalized by total height of the building), and member plastic end rotations for the six-story building excited by 30 records. In addition to mean (50 percentile) demands, the 16 and 84 percentile demands are also marked. Each response parameter shows considerable record-to-record variation. In general, significant yielding concentrates at the first story level, while some records impose enhanced displacement demands at the upper levels by triggering higher mode effects. Peak value of mean IDR is close to 2% at the first story level. As mentioned earlier, for this structure yielding at the first story level starts as early as 0.8% IDR. At the end of each NTH run, the ECE demand of the MDOF system was computed by utilizing Eq. 12. Estimates of these demands are then computed using the elastic ECE spectrum based on the modal decomposition given by Eq. 11 and considering the first three elastic modal properties (i.e., T_n, Γ_n) of the building. Figure 15a presents the comparison of computed and estimated ECE demands. The data is closely scattered around the diagonal reference line (not the best-fit line) indicating the reliability of the procedure. Some dispersion in the estimates is observed at higher energy levels, which could be possibly reduced if inelastic ECE spectra were utilized. Figure 15b,c provides an example of correlating MDOF system performance with ECE demand. In this figure, the

TABLE 2 Selected 30 near-fault recordings for ECE estimation through modal-energy decomposition

No.	Year	Earthquake	Station
1	1984	Morgan Hill	Anderson Dam
2	1979	Imperial-Valley	Brawley Airport
3	1979	Imperial-Valley	El Centro Array #3
4	1979	Imperial-Valley	El Centro Diff. Array
5	1979	Imperial-Valley	El Centro Imp. Co. Cent.
6	1979	Imperial-Valley	Holtville Post Office
7	1999	Kocaeli	Duzce
8	1989	Loma Prieta	Gilroy STA #2
9	1989	Loma Prieta	Gilroy STA #3
10	1994	Northridge	Rinaldi Rec. Stn.
11	1994	Northridge	Slymar Converter Sta East
12	1992	Cape Mendocino	Petrolia, General Store
13	1979	Imperial-Valley	El Centro Array #7
14	1994	Northridge	Jensen Filt. Plant
15	1984	Morgan Hill	Coyote Lake Dam
16	1994	Northridge	Newhall LA Fire Stn.
17	1994	Northridge	Sylmar Olive View Hospital
18	1994	Northridge	Newhall Pico Canyon
19	1987	Superstition Hills	Parachute Test Site
20	1992	Erzincan	Erzincan
21	1989	Loma Prieta	Corralitos
22	1999	Chi-Chi	TCU052
23	1999	Chi-Chi	TCU068
24	1999	Kocaeli	Yarimca
25	1999	Kocaeli	Yarimca
26	1999	Chi-Chi	TCU067
27	2004	Parkfield	Cholame 1E
28	2004	Parkfield	Cholame 5W (Sta 5)
29	2004	Parkfield	Fault Zone 1
30	2004	Parkfield	Gold Hill 1 W

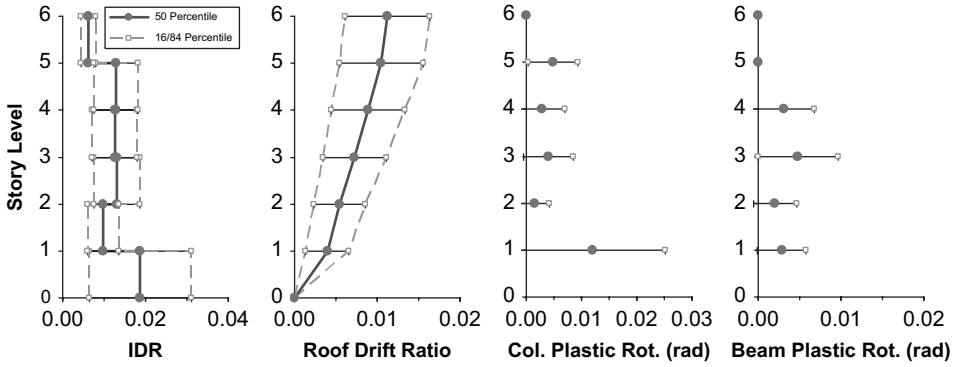

FIGURE 14 Height-wise statistical variation of NTH analyses' results of six-story building excited by 30 near-fault records.

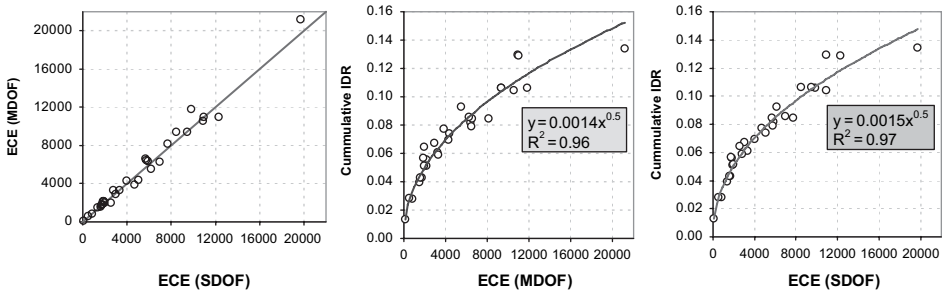

(a) (b) (c)

FIGURE 15 (a) ECE estimates based on ECE spectrum and modal energy decomposition approach; (b) relation between cumulative IDR and computed ECE (through MDOF system); (c) relation between cumulative IDR and estimated ECE. (Note: ECE is given in units of k-in).

peak value of cumulative IDR, is plotted against ECE computed by MDOF formulation and then the same response parameter is plotted against ECE estimates via modal energy decomposition (Figure 15c). Cumulative IDR (independent sum of peak IDR of each story) is selected herein as a representative single-valued performance parameter, since it potentially provides insight into the level of average distributed deformation through the height of the structure. Although the peak IDR of each story does not necessarily takes place at the same time instant, we have shown previously in Figure 11 and also in another study [Kalkan and Kunnath, 2007b] that peak response values are well-synchronized with the arrival of dominant pulse contained in the ground motion which also corresponds to the time period in which the ECE is computed. Data in Figures 15b and 15c is best correlated by a power function, which yields a high correlation coefficient (i.e., $\sqrt{R^2}$) exceeding 0.98. The other response parameters such as peak roof drift ratio and peak IDR when plotted against ECE provided virtually identical results and therefore are not included here.

As indicated in Figures 6 and 7, increase in the ECE of a SDOF oscillator results in linearly amplified displacement demand. However, this relation is found to be parabolic for the MDOF system when the cumulative IDR is considered as a response parameter. The most important observation is that the equations as shown in Figures 15b and 15c that relate a particular response parameter to actual and predicted ECE are almost identical. Initiating such a relation between ECE and other response parameters provides invaluable opportunities. As such, the backbone curve plotted in Figure 15b,c can be considered as energy-capacity diagram (analogous to classical capacity curve) which potentially indicates level of drift demands created in the structure by the records having varying intensity level. Once such an equation is computed for a specific structure, it can be effectively used for direct performance evaluation without performing NTH analysis instead using ECE spectrum of a pulse-type record and modal energy decomposition. The implementation of this new approach in performance-based design and assessment is currently underway.

7. Conclusions

It is well known that the ability of structural components to dissipate energy through viscous and hysteretic damping is a primary factor contributing to structural damage during earthquakes. For far-fault records, this damage is a direct consequence of the number and amplitude of plastic deformation cycles. Hence, in quantifying the damage potential of

ground motions, it is important to include the cyclic effects over the duration of strong ground shaking. In contrast, near-fault ground motions often have an impulsive feature and impose sudden and intense energy input that should be dissipated within a short period of time. This causes amplified deformation demands in structures and is associated with very few cycles of plastic deformation and, therefore, earthquake damage is related to the maximum deformation or maximum ductility. While most of the previous studies on energy demand have focused on far-fault records (or a collection of records in which ground motion characteristics were not explicitly considered), the present research is concerned primarily with near fault records. It is demonstrated that peak deformation is well correlated to effective cyclic energy (ECE), and a relationship between ECE and maximum deformation is proposed through a severity index (γ_{eff}). This non dimensional index can be used to include displacement parameters in seismic design procedures based on energy concepts, and also to assess the damage potential of ground motions. Since ECE is influenced by system response, the development of ECE spectra is shown to be more appropriate than conventional acceleration spectra to assess deformation demands in structures.

Finally, a procedure utilizing the modal-energy-decomposition through elastic ECE spectrum is presented to estimate the ECE demand of MDOF systems whereby "modal-target-energy" demands are computed to be used directly in performance evaluations without performing NTH analysis. The proposed procedure is validated for an instrumented moment frame building for a large set of forward directivity and fling records, and satisfactory energy estimates are obtained. ECE is also shown to be a stable parameter and well correlated with computed structural response parameters such as peak values of cumulative IDR, IDR, and peak roof displacement even at high inelasticity levels. These findings suggest that ECE can potentially be used as a single descriptor to quantify the local and overall displacement demand parameters once the interrelation between them and ECE is constructed (a sample formulation was presented in Figure 15c).

The features of ECE presented in this paper indicate that it can be a valuable tool in developing energy-based guidelines for performance assessment of building structures when near-fault ground motions effects on structures are a primary concern.

Acknowledgments

Funding for this study provided by the National Science Foundation under Grant CMS-0296210, as part of the US-Japan Cooperative Program on Urban Earthquake Disaster Mitigation, is gratefully acknowledged. Any opinions, findings, and conclusions or recommendations expressed in this material are solely those of the authors and do not necessarily reflect the views of the National Science Foundation. We would also like to thank two anonymous reviewers, their suggestions helped improving the paper.

References

American Society of Civil Engineers (ASCE), [2000]. *Prestandard and Commentary for the Seismic Rehabilitation of Buildings*, FEMA-356, Washington D.C.

Amiri, G. G. and Dana, F. M. [2005]. "Introduction of the most suitable parameter for selection of critical earthquake," *Computers & Structures*, **83**(8–9), 613–26.

Applied Technology Council (ATC) [1996]. *Seismic Evaluation and Retrofit of Concrete Buildings*, Volumes 1 and 2, Report No: ATC-40, Redwood City, CA.

Applied Technology Council (ATC) [2005]. "FEMA-440: Improvement of nonlinear static seismic analysis procedures," Prepared by ATC (ATC-55 Project) for FEMA, Washington D.C.

Boore, D. M., Joyner, W. B., and Fumal, T. E. [1997]. "Equations for estimating horizontal response spectra and peak acceleration from western North American earthquakes: A summary of recent work," *Seismology Research Letters*, **68**, 128–153.

Boore, D. M. [2001]. "Effect of baseline corrections on displacements and response spectra for several recordings of the 1999 Chi-Chi, Taiwan, earthquake," *Bulletin of the Seismological Society of America*, **91**(5), 1199–1211.

Bray, J. D. and Rodriguez-Marek, A. [2004]. "Characterization of forward-directivity ground motions in the near-fault region," *Soil Dynamics and Earthquake Engineering*, **24**, 815–828.

Chopra A. K. and Chintanapakdee C. [2001]. "Comparing response of SDF systems to near-fault and far-fault earthquake motions in the context of spectral regions," *Earthquake Engineering & Structural Dynamics*, **30**(2), 1769–1789.

Chintanapakdee, C. and Chopra, A. K. [2003]. "Evaluation of modal pushover analysis using generic frames," *Earthquake Engineering and Structural Dynamics*, **32**(3), 417–442.

Chou, C. C. and Uang, C. [2003]. "A procedure for evaluating seismic energy demand of framed structures," *Earthquake Engineering and Structural Dynamics*, **32**, 229–44.

Decanini, L. D. and Mollaioli, F. [2001]. "An energy-based methodology for the assessment of seismic demand," *Soil Dynamics and Earthquake Engineering*, **21**(2), 113–37.

Fajfar, P. [1992]. "Equivalent ductility factors, taking into account low-cycle fatigue," *Earthquake Engineering and Structural Dynamics*, **23**, 507–21.

Fajfar, P. and Vidic, T. [1994]. "Consistent inelastic design spectra: hysteretic and input energy," *Earthquake Engineering and Structural Dynamics*, **23**, 523–37.

Gupta, B. and Kunnath, S. K. [1998]. "Effect of hysteretic model parameters on inelastic seismic demands," *Proceedings of 6th US National Conference on Earthquake Engineering*, Seattle, WA.

Hernandez-Montes, E., Kwon, O. S., and Aschheim, M. A. [2004]. "An energy based formulation for first and multiple-mode nonlinear static (Pushover) analyses," *Journal of Earthquake Engineering*, **8**(1), 69–88.

Kalkan, E. [2006]. *Prediction of seismic demand in building structures*, Ph.D. Dissertation, University of California at Davis.

Kalkan, E. and Gülkan, P. "Site-dependent spectra derived from ground motion records in Turkey," *Earthquake Spectra*, **20**(4), 1111–1138.

Kalkan, E. and Kunnath, S. K. [2006a], "Effects of fling-step and forward directivity on the seismic response of buildings," *Earthquake Spectra*, **22**(2), 367–390.

Kalkan, E. and Kunnath, S. K. [2006b]. "Adaptive modal combination procedure for nonlinear static analysis of building structures," *Journal of Structural Engineering*, ASCE, **132**(11), 1721–1732.

Kalkan, E. and Kunnath, S. K. [2007a]. "Relevance of absolute and relative energy content in seismic evaluation of structures," *Advances in Structural Engineering*. (in press).

Kalkan, E. and Kunnath, S. K. [2007b]. "Assessment of current nonlinear static procedures for seismic evaluation of buildings," *Engineering Structures*. **29**(3), 305–316.

Kunnath, S. K. and Kalkan, E. [2004]. "Evaluation of seismic deformation demands using nonlinear procedures in multistory steel and concrete moment frames," *ISET, Journal of Earthquake Technology* (Special Issue on Performance Based Design), **41**(1), 159–181.

Kunnath, S. K. and Chai, R. Y. H. [2004]. "Cumulative damage-based inelastic cyclic demand spectrum," *Earthquake Engineering and Structural Dynamics*, **33**, 499–520.

Kunnath, S. K. Nghiem, Q., and El-Tawil, S. [2004]. "Modeling and response prediction in performance-based seismic evaluation: case studies of instrumented steel moment-frame buildings," *Earthquake Spectra*, **20**(3), 883–915.

Kuwamura, H. and Galambos, T. V. [1989]. "Earthquake load for structural reliability," *Journal of Structural Engineering*, ASCE, **115**, 1446–62.

Mavroeidis, G. P. Dong, G., and Papageorgiou, A. S. [2004]. "Near-fault ground motions, and the response of elastic and inelastic single-degree-freedom (SDOF) systems," *Earthquake Engineering and Structural Dynamics*, **33**, 1023–1049.

Lawson, R. S. and Krawinkler, H. [1995]. "Cumulative damage potential of seismic ground motion," *Proc. of the 11th World Conference on Earthquake Engineering*, Wien, Balkema, pp. 1079–86.

OpenSees [2006]. Open system for earthquake engineering simulation, (available online), URL: http://opensees.berkeley.edu.

Ramirez, O. M., Constantinou, M. C. Whittaker, A. S. Kircher, C. A., and Crysostomou C. Z. [2002]. "Elastic and inelastic seismic response of buildings with damping systems," *Earthquake Spectra*, **18**(3), 531–547.

Riddell, R. and Garcia, E. J. [2001]. "Hysteretic energy spectrum and damage control," *Earthquake Engineering and Structural Dynamics*, **30**, 1791–1816.

Ruiz-Garcia, J. and Miranda, E. [2003]. "Inelastic displacement ratios for evaluation of existing structures," *Earthquake Engineering & Structural Dynamics*, **32**, 1237–1258.

Spacone, E., Ciampi, V., and Filippou, F. C. [1992] "A beam element for seismic damage analysis," Report No. UCB/EERC-92/07, Earthquake Engineering Research Center, University of California, Berkeley.

Sucuoglu, H., Yucemen, S., Gezer, A., and Erberik, A. [1998]. "Statistical evaluation of the damage potential of earthquake ground motions," *Structural Safety*, **20**, 357–378.

Sucuoglu, H. and Erberik, A. [2004]. "Energy-based hysteresis and damage models for deteriorating systems," *Earthquake Engineering and Structural Dynamics*, **33**, 69–88.

Teran-Gilmore, A. 1998. "A parametric approach to performance-based numerical seismic design," *Earthquake Spectra*, **14**(3), 501–520.

Teran-Gilmore, A. and Jirsa, J. O. [2005]. "A damage model for practical seismic design that accounts for low cycle fatigue," *Earthquake Spectra*, **21**(3), 803–832.

Trifunac, M. D. and Brady, A. G. [1975]. "On the correlation of seismic intensity scales with the peaks of recorded ground motion," *Bulletin of the Seismological Society of America*, **65**, 139–62.

Uang, C. M. and Bertero, V. V. [1990]. "Evaluation of seismic energy in structures," *Earthquake Engineering and Structural Dynamics*, **19**, 77–90.